AGU PUBLICATIONS

Geophysical Research Letters

RESEARCH LETTER
10.1002/2017GL073726

Key Points:
- Ultrasonic velocities are measured in the laboratory to quantify anisotropy due to rock fabric in phyllosilicate-rich Carboneras fault
- Compressional and shear wave velocities show anisotropy of 10–15% in the Carboneras fault gouge and 35–50% in the mica-schist protolith
- The degree and orientation of seismic anisotropy with respect to a fault may be a key consideration in seismic imaging of the fault

Supporting Information:
- Supporting Information S1

Correspondence to:
C. M. Kelly,
cmkelly@liv.ac.uk

Citation:
Kelly, C. M., D. R. Faulkner, and A. Rietbrock (2017), Seismically invisible fault zones: Laboratory insights into imaging faults in anisotropic rocks, *Geophys. Res. Lett.*, *44*, 8205–8212, doi:10.1002/2017GL073726.

Received 10 APR 2017
Accepted 31 JUL 2017
Accepted article online 3 AUG 2017
Published online 16 AUG 2017

Seismically invisible fault zones: Laboratory insights into imaging faults in anisotropic rocks

C. M. Kelly[1], D. R. Faulkner[1], and A. Rietbrock[1]

[1]Department of Earth, Ocean and Ecological Sciences, University of Liverpool, Liverpool, UK

Abstract Phyllosilicate-rich rocks which commonly occur within fault zones cause seismic velocity anisotropy. However, anisotropy is not always taken into account in seismic imaging and the extent of the anisotropy is often unknown. Laboratory measurements of the velocity anisotropy of fault zone rocks and gouge from the Carboneras fault zone in SE Spain indicate 10–15% velocity anisotropy in the gouge and 35–50% anisotropy in the mica-schist protolith. Greater differences in velocity are observed between the fast and slow directions in the mica-schist rock than between the gouge and the slow direction of the rock. This implies that the orientation of the anisotropy with respect to the fault is key in imaging the fault seismically. For example, for fault-parallel anisotropy, a significantly greater velocity contrast between fault gouge and rock will occur along the fault than across it, highlighting the importance of considering the foliation orientation in design of seismic experiments.

1. Introduction

Identifying faults is an important step toward understanding fault mechanics and is crucial in accurately and reliably assessing seismic hazard. Seismic hazard was reevaluated after the discovery of the Greendale fault, New Zealand, following the 2010 Darfield earthquake [e.g., *Quigley et al*., 2012] and in Haiti following the *M*7.0 earthquake on the previously unmapped Léogâne fault [e.g., *Calais et al*., 2010].

Seismic investigations are often conducted in order to understand the fault structure at depth. Subhorizontal and dipping faults have been observed as major reflectors in seismic reflection images of the crust, and an increase in velocity with depth in the crust allows reflections of near-vertical faults to be detected in surface seismic surveys [e.g., *Hole et al*., 1996]. Faults are also identified in seismic refraction surveys from vertical offsets in velocity profiles and distinctive features in the seismic arrivals caused by low velocities, velocity contrasts across the fault and fault zone head waves [e.g., *Yan et al*., 2005]. Tomographic studies can image the area around a fault zone [e.g., *Thurber et al*., 2006] and may indicate the extent of fracturing and damage [e.g., *Lin and Shearer*, 2009]. However, narrow structures such as individual fault strands may not be resolved. The imaging resolution may be improved by adding travel time information of phases that spend much of their travel path along the fault zone structure [e.g., *Ben-Zion et al*., 1992].

The detailed structure of faults has been investigated through fault zone guided waves. Guided waves result from coherent multiple reflections at the boundaries between a low-velocity fault zone and higher-velocity surrounding rock. These waves can probe the internal structure and continuity of the fault zone at depth [*Ben-Zion*, 1998; *Peng et al*., 2003]. Guided waves have been used to resolve fault zone widths of tens to several hundreds of meters [e.g., *Li et al*., 1990]. Observations of guided waves rely on a significant velocity contrast, provided by a low-velocity damage zone relative to the protolith, or contrasts between the fault core and damage zone.

Seismic anisotropy is frequently observed in fault zones and has been studied extensively using seismological techniques including shear wave splitting observations [e.g., *Cochran et al*., 2003] and anisotropy tomography [*Zhang et al*., 2007; *Lin et al*., 2014]. Where shear wave splitting is observed in fault zones, fast directions are often determined to be between the regional maximum compressive stress direction and fault parallel and may change as the strike of the fault changes [e.g., *Cochran et al*., 2003; *Liu et al*., 2004; *Cochran and Kroll*, 2015]. In Chi-Chi, Taiwan, and Hector Mine, California, the anisotropic area around the fault zone is observed to be of the order of 1 km wide [*Cochran et al*., 2003] and is often inferred to extend no more than a few kilometers in depth [e.g., *Savage et al*., 1990]. Anisotropy in fault zones is often inferred to result from a preferred fracture orientation due to the surrounding stress field [e.g., *Evans*, 1984]. Foliation or aligned minerals can also contribute to anisotropy within a region [*Aster and Shearer*, 1992].

Many faults occur within phyllosilicate-rich rocks, e.g., the San Andreas Fault in California, Alpine fault in New Zealand, and Median Tectonic Line in Japan [e.g., *Moore and Rymer*, 2007; *Christensen and Okaya*, 2007; *Jefferies et al*., 2006]. Phyllosilicate-rich rocks by their very nature display a pervasive anisotropic fabric. This fabric can cause velocity anisotropy [e.g., *Dempsey et al*., 2011]. However, strong anisotropy is often unaccounted for in seismic imaging. The presence of anisotropy can cause serious artifacts in tomography if isotropy is assumed [e.g., *Chapman and Pratt*, 1992]. Modeling of guided wave observations has so far been based on relatively simple layered structures, and although numerical studies of guided waves have considered some of the effects of complex fault geometries [e.g., *Igel et al*., 2002], greater consideration should be given to the effects of strong seismic anisotropy [e.g., *Gulley et al*., 2017].

We use laboratory measurements on the Carboneras fault zone, a major regional strike-slip fault in SE Spain, to consider the potential effect of anisotropy on seismic imaging. The onshore portion of the fault zone has been mapped extensively [*Faulkner et al*., 2003; *Rutter et al*., 2012]. The region is experiencing active uplift; the fault has been exhumed from depth of 1.5–4 km during the past 10 Ma. The climate is now semiarid, and as a result, the fault is well exposed and the fault rocks are extremely well preserved [*Faulkner et al*., 2003]. The fault rocks exposed at the surface today are primarily derived from the metamorphic basement, dominated by mica-schist of the Nevado Filabride complex which becomes the primary protolith at depth [*Faulkner et al*., 2003].

In this paper ultrasonic velocity measurements through gouge from the Carboneras fault and the phyllosilicate-rich mica-schist from intact country rock which surrounds the fault zone are presented. This allows quantification of the extent of velocity anisotropy present in this phyllosilicate-rich fault due to the rock fabric. It is postulated that the orientation of a seismic experiment with respect to anisotropic geological fabric may be key in successfully imaging a fault zone. Where a fault is imaged successfully with a guided wave experiment it may not necessarily be imaged successfully with reflection or refraction experiments (or vice versa).

2. Methodology

Ultrasonic velocities are measured at a range of effective pressures across samples of fault gouge and mica-schist rock of the Nevado-Filabride complex of SE Spain from which it is derived. The mica-schist rock is transversely isotropic with one strong foliation and isotropy within the plane of the foliation. Rock samples were drilled perpendicular and parallel to the foliation of the mica-schist in the laboratory (see Figure 1). The fault gouge displays internal structuring showing P/R_1 foliation, where P foliation is defined by the preferred alignment of phyllosilicates in a plane oblique to the direction of shear and R_1 shears by a sense of obliquity opposite to that of the P foliation [*Rutter et al*., 1986]. Gouge samples were collected by hammering a copper tube into the fault gouge [e.g., *Faulkner and Rutter*, 1998]. Three perpendicular orientations were sampled: perpendicular to the fault plane, in the transport direction of the fault, and the direction perpendicular to this within the fault plane. Further details of sample characterization, sample preparation, and experimental setup and procedure can be found in the supporting information. No pore fluids were introduced and both compressional and shear wave velocities were measured.

Two different types of experiment are carried out on the mica-schist rock. First, velocities are measured at confining pressures up to 80 MPa with no axial load applied. This allows changes in velocity and velocity anisotropy with increasing depth to be established. Assuming a pressure gradient of approximately 25 MPa/km, these confining pressures represent approximately the upper 3 km of the crust. Second, cyclic loading experiments were carried out. In these, a sample is held at a fixed confining pressure of 25 MPa (corresponding to a depth of approximately 1 km) and axial loading is applied. A sample is taken to 40% of its expected failure stress, and on increasing cycles the sample is taken closer to the failure stress and then unloaded after failure [e.g., *Heap and Faulkner*, 2008]. With each cycle, the higher stress is expected to induce microcrack damage. This technique allows separation of the effects of loading conditions and microcrack damage on the measured velocity, as measurements can be made at similar loading conditions on each cycle. It is well established that fracture density increases with decreasing distance to the fault core [e.g., *Mitchell and Faulkner*, 2009]. Therefore, each sequential loading cycle essentially simulates the stress state that the damage zone experiences from intact (undamaged) country rock to highly damaged rock as the fault core is approached.

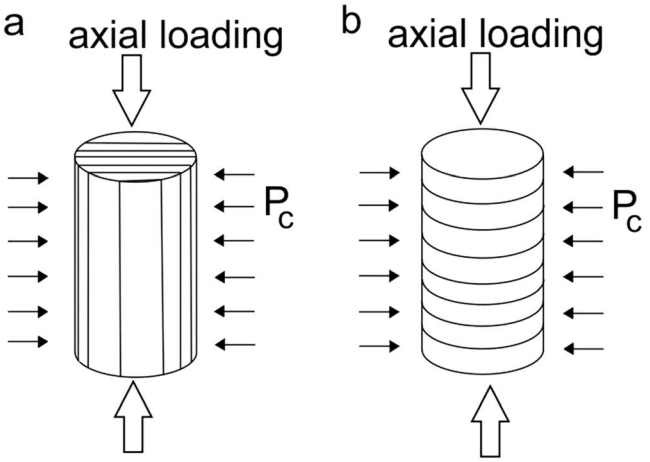

Figure 1. Samples cored (a) parallel and (b) perpendicular to the foliation are shown schematically, with foliation indicated. Ultrasonic velocity measurements are made axially across samples. In all experiments presented, confining pressure (P_c) is applied.

Velocities are measured through the fault gouge at confining pressures up to 60 MPa, allowing velocity changes with increasing depth to be established.

It is noted that frequencies used in the laboratory experiments presented are of the order of 1 MHz, whereas frequencies used in seismic investigations are generally less than or around 100 Hz. However, the observed fabric responsible for the anisotropy is pervasive throughout the protolith and so can also be expected to cause velocity anisotropy at seismic frequencies. It is well recognized that anisotropy of small-scale features can exert an important influence at seismic wavelengths [e.g., *Crampin*, 1978; *Kaarsberg*, 1959], and measurements have been successfully compared across different wavelengths [e.g., *Crampin*, 1994].

3. Results

Throughout the experiments, the foliation in the mica-schist is observed to have a strong effect on the measured velocities. In the hydrostatic experiments, in the sample cored parallel to the foliation, compressional wave velocities are observed to increase from 5200 ms^{-1} to 5600 ms^{-1} and shear wave velocities from 3400 ms^{-1} to 3700 ms^{-1} with increasing confining pressure (see Figure 2). This can be interpreted as crack closure with increasing pressure. In the sample cored perpendicular to the foliation, compressional wave velocities increase from 3000 to 3900 ms^{-1} and shear wave velocities from 2300 ms^{-1} to 2600 ms^{-1} with increasing confining pressure (see Figure 2). Up to confining pressures of at least 80 MPa, significant differences are observed in the velocities measured in different sample orientations. The measured velocities correspond to compressional wave anisotropy of 40–50% and shear wave anisotropy of 35%, with percentage anisotropy defined as $100\left(\frac{\max V - \min V}{\overline{V}}\right)$.

Gouge velocities are slower than those through the mica-schist rock samples (Figure 3). The measured compressional wave velocities in the gouge are 40–50% less than those measured through the rock samples

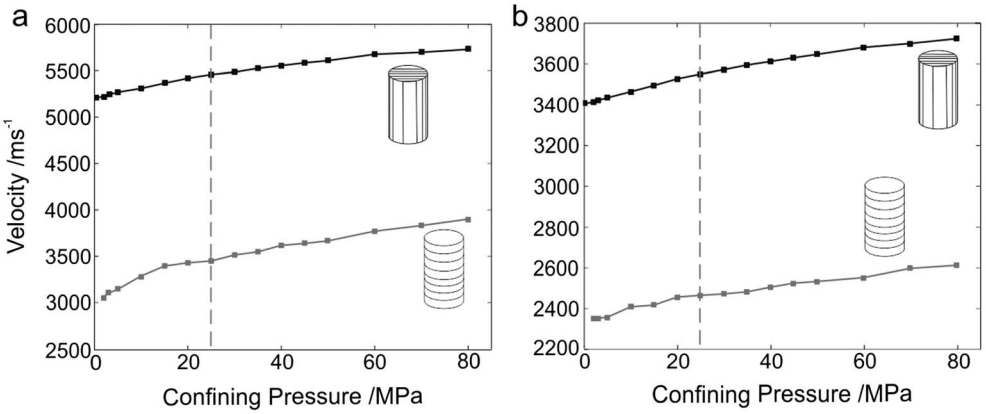

Figure 2. Characterizing the protolith velocities. (a) Compressional wave and (b) shear wave velocities measured with increasing confining pressure through samples cored parallel to the foliation (black line) and perpendicular to the foliation (grey line,). Dashed line represents measurements at 25 MPa, used in Figures 4 and 5.

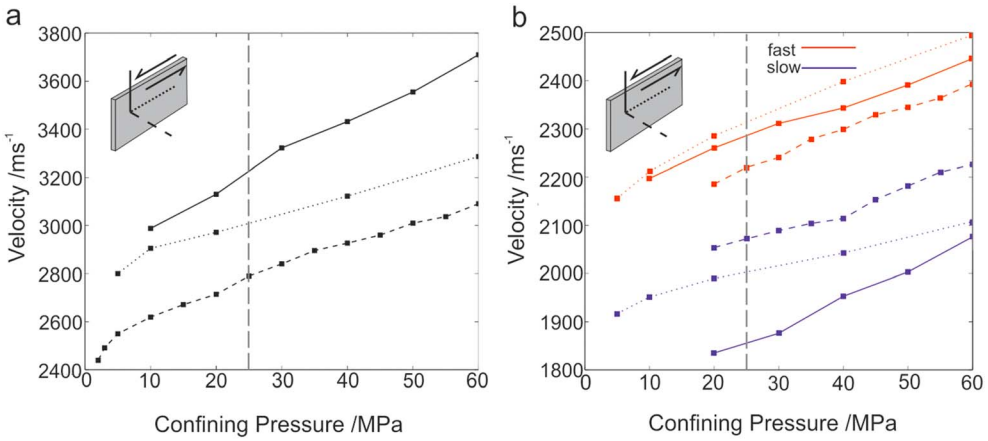

Figure 3. Fault gouge velocity anisotropy measurements. (a) Compressional wave and (b) shear wave velocities through the gouge are measured in three perpendicular directions: perpendicular to the fault plane (dashed line), in the transport direction of the fault (dotted line), and in the fault plane, perpendicular to the transport direction of the fault (solid line).

parallel to the foliation or 5–20% less than those through the perpendicular rock samples. Shear wave velocities in the gouge are 30–40% less than those measured through the rock samples parallel to the foliation or 5–20% less than those through the perpendicular rock samples. Anisotropy of 10–15% is apparent in the compressional wave and shear wave velocities measured through the fault gouge. This anisotropy most likely represents the internal structure of the fault gouge [*Rutter et al*., 1986]. Anisotropy has also previously been observed in permeability measurements of this fault gouge [*Faulkner and Rutter*, 1998].

Velocity changes measured in the mica-schist rock due to cyclic loading are less than 5% of the original velocity and suggest that limited velocity reduction occurs within the fault damage zone in these types of rocks (Figure 4). Larger-scale observations at the Alpine Fault, New Zealand, also do not show an increase in the density of fault damage zone structures within the phyllosilicate rocks close to the fault core [*Williams et al*., 2016]. These observations contrast with the large changes in elastic properties measured in crystalline rocks such as granite and basalt using similar methods as presented here [e.g., *Heap and Faulkner*, 2008].

There may be greater velocity changes within the damage zone at larger length scales. In comparing velocity measurements between laboratory, sonic log and seismic scales for the San Andreas Fault, *Jeppson and Tobin* [2015] found that although velocities were relatively consistent across the length scales for both gouge and

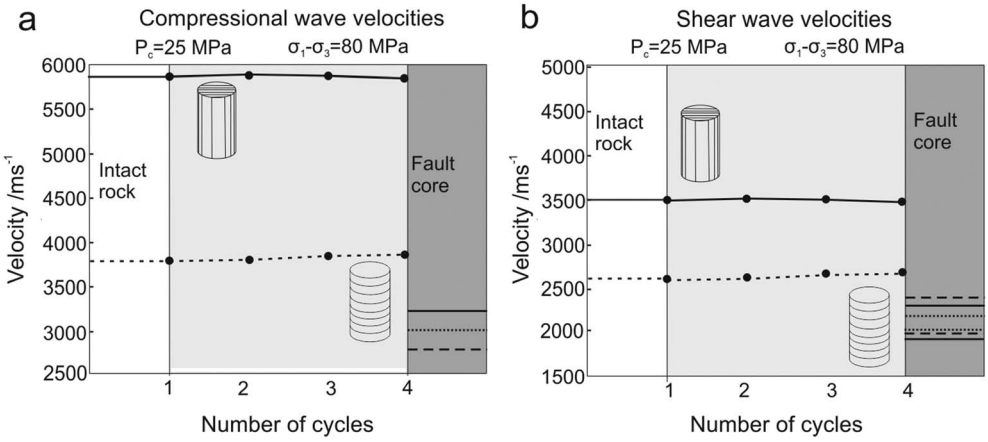

Figure 4. Summary of measurements to characterize the effect of cyclic loading on measured velocities. For a confining pressure of 25 MPa and differential stress of 80 MPa, (a) compressional wave and (b) shear wave velocities measured on increasing cycles are shown. Increasing cycles are expected to increase damage and may act as a proxy to moving toward the fault core. Fault gouge velocities are also shown. For further information, see supporting information Figure S2.

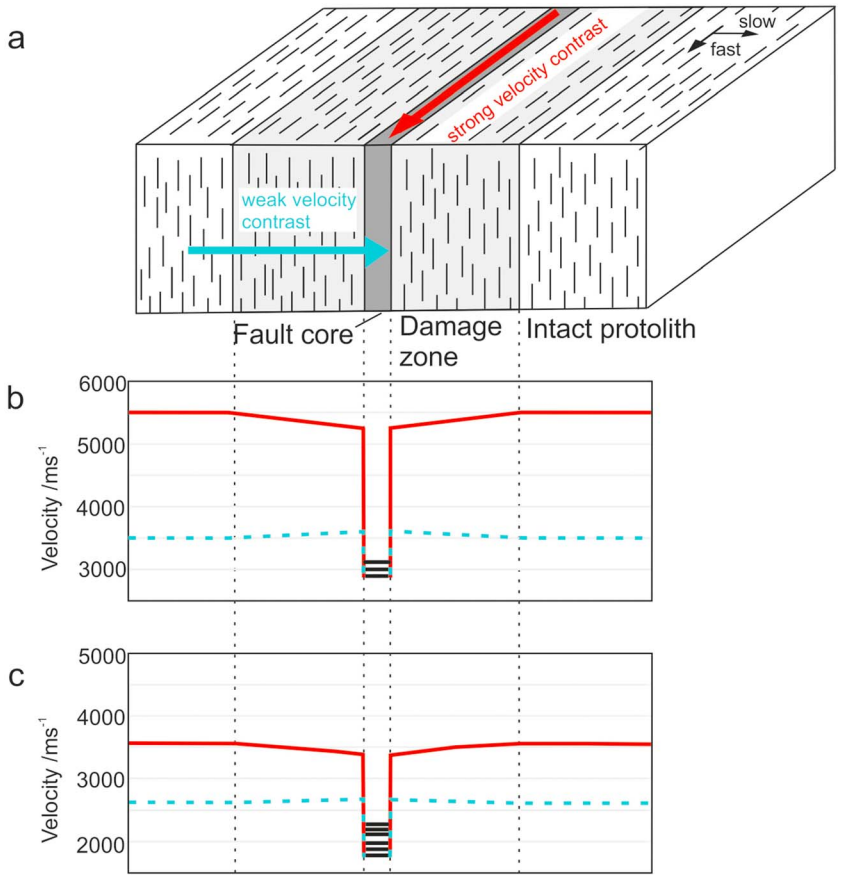

Figure 5. For a single fault strand surrounded by damaged country rock, as shown schematically in (a), the (b) compressional and (c) shear wave velocities measured in the laboratory at confining pressure of 25 MPa (corresponding to a depth of approximately 1 km) are summarized. Dotted lines indicate how the velocities presented correspond to the fault core (measurements through fault gouge, Figure 3), fracture damage zone (measurements made in cyclic loading experiments, Figure 4), and intact rock (measurements through the protolith at confining pressure, Figure 2). In Figures 5b and 5c the solid red line represents measurements made in the micashist parallel to the foliation, indicated as a raypath along the fault for fault-parallel anisotropy. The dashed blue line represents velocity measurements made perpendicular to the foliation, indicated as a raypath across the fault for fault-parallel anisotropy.

undamaged country rock, laboratory estimates of damage zone rocks were 9 to 41% higher than sonic log measurements. They attributed this to the effects of macroscale deformation features and a necessary bias in laboratory sampling requiring intact rock. Velocity measurements by *Taylor et al*. [2015] through Carboneras fault gouge indicate similar velocities at a separate locality, indicating that the results here are generally applicable for this fault. Their measurements through graphitic mica-schist also indicate a similar degree of anisotropy at similar pressures and confirm that strong anisotropy persists within the mica-schist to greater pressures (27% anisotropy at 200 MPa). Measurements of fault rock permeability from numerous localities along the Carboneras fault have shown a remarkable degree of consistency, implying homogeneity of the fault rock in this region [*Faulkner and Rutter*, 1998, 2000, 2001]. Velocities measured in the laboratory for the Carboneras fault zone have also previously been compared to those measured in field seismic surveys by *Taylor et al*. [2015], with good agreement at pressures of about 2 MPa (corresponding to depths of approximately 80 m).

4. Discussion

Using the data set collected, an image of the likely velocity structure at shallow depths around faults in foliated schistose terranes can be constructed (Figure 5). Strong velocity anisotropy, as measured in this study, will have significant influence on seismic imaging of faults. Relatively small velocity changes are measured due to cyclic loading of samples, suggesting relatively small changes of velocity in the fault damage

zone compared with the intact country rock. Velocities through the fault gouge are slower than through the mica-schist rock. Based on laboratory velocities, strands of fault gouge will form low-velocity structures, as has been seen in faults of similar composition, e.g., Parkfield area of the San Andreas Fault.

Sample ultrasonic measurements were made on dry samples, but fault zones in the subsurface are generally expected to be saturated. Any differences in velocity due to saturation are likely to be less than 10% [*Ghorbani et al*., 2009] and are not expected to alter our main conclusions.

A key observation is that greater differences in velocity are observed between the fast and slow directions in the mica-schist rock, than between the gouge and the slow direction of the rock. Therefore, the orientation of the foliation with respect to the fault and the geometry of a seismic experiment can have important effects on the successful imaging of the fault (see Figure 5).

When foliation is oriented parallel to a fault, a guided wave will be sensitive to the large velocity contrast between the fault gouge and the fast direction of the rock. However, in the same circumstances, waves traveling along a raypath perpendicular to the fault will sample the much smaller velocity contrast between gouge and the slow direction in the rock (see Figure 5).

If the orientation of the foliation changes along the strike of the fault, as it is reported along the Carboneras fault [*Rutter et al*., 2012], then the velocity contrast and reflection coefficient may also change. This may lead to energy leakage for a guided wave traveling along the fault zone.

Relatively large changes in the orientation of the foliation over short distances, e.g., due to folding, will also influence seismic images. For a seismic profile across the fault, if foliations are vertical near a fault strand and shallow laterally away from the fault due to folding, then the greatest velocity contrast could potentially be due to the change in orientation of the foliation, rather than the strand of fault gouge within the rock. In this case the fault strand may not appear and areas of reduced velocity may be caused by large changes in foliation orientation over short distances. This emphasizes the importance of considering geological observations where available.

Strong velocity anisotropy due to rock fabric is not unique to the Carboneras fault zone, and there are many examples of faults in anisotropic rock. *Christensen and Okaya* [2007] report velocity measurements from a range of rock types from the South Island, New Zealand. Measurements indicate high-velocity anisotropy across many rock types (typically 30–40% anisotropy but up to 70% anisotropy). They conclude that seismic anisotropy is a pervasive feature throughout much of the South Island crust, where many faults exist. This strong anisotropy may explain, for example, why guided wave studies of the Alpine Fault have indicated a 10–40% velocity reduction, whereas refraction studies have implied a much smaller velocity reduction of 4–16% and the fault has been imaged as a weak reflector [*Eccles et al*., 2015; *Davey*, 2010; *Eberhart-Phillips and Bannister*, 2002].

Other faults occurring within phyllosilicate-rich rocks may exhibit similar characteristics. Using teleseismic receiver functions, *Audet* [2015] observe strong, layered anisotropy ($>$30% in the upper 5–10 km) surrounding the San Andreas Fault near Parkfield, interpreted as foliation and fluid-filled microcracks. Strong anisotropy may also occur in fault zones where phyllosilicate material is not a major component. Stress-induced anisotropy is often observed in fault zones [e.g., *Liu et al*., 2004; *Cochran and Kroll*, 2015]. If the extent of stress-induced anisotropy is significant, then this may also affect seismic imaging of faults in a similar way.

If attempting to image a fault in anisotropic rocks, the success of a seismic experiment can be maximized by establishing the orientation of any strong geological fabric (e.g., foliation) with respect to the fault, and how this orientation changes along the strike of the fault and at distances away from the fault. Laboratory measurements, such as those presented, may help to establish the extent of velocity anisotropy contributed by a geological fabric. How this geological fabric may affect the identification of regional faults can then be considered. If there is a consistently oriented strong fabric then it may be relatively simple to establish the best geometry for a seismic experiment. In order to image successfully the fault, the greatest velocity contrast should be sampled, e.g., a guided wave experiment for fast direction parallel to the fault.

It is also important to consider if anisotropy changes with depth, e.g., from detailed structural mapping, cores from drilling, or previous geophysical surveys. Suspected changes in anisotropy orientation with depth [e.g., *Audet*, 2015] may require numerical modeling in order to establish the best geometry for a successful seismic

survey. Similarly, if there is more than one source of anisotropy (e.g., anisotropy due to fractures parallel to the fault as well as foliation), then further investigation may be warranted prior to embarking on a seismic survey and numerical modeling may be carried out to determine the optimum geometry in which to image any faults.

Throughout these experiments, the strong influence of anisotropic fabric on velocities measured has been shown. The effects that significant anisotropy will have on seismic images will depend on the geometry of the seismic investigation. The influences of anisotropy on seismic investigations need to be determined for specific source-receiver geometries and the local geological fabric as strong anisotropy may lead to poorly imaged fault structures.

Acknowledgment
Research was supported by NERC grant NE/F019920/1. The data used are displayed in figures and in the supporting information.

References

Aster, R., and P. Shearer (1992), Initial shear wave particle motions and stress constraints at the Anza seismic network, *Geophys. J. Int.*, *108*, 740–748.

Audet, P. (2015), Layered crustal anisotropy around the San Andreas Fault near Parkfield, California, *J. Geophys. Res. Solid Earth*, *120*, 3527–3543, doi:10.1002/2014JB011821.

Ben-Zion, Y. (1998), Properties of seismic fault zone waves and their utility for imaging low-velocity structures, *J. Geophys. Res.*, *103*, 12,567–12,585, doi:10.1029/98JB00768.

Ben-Zion, Y., S. Katz, and P. Leary (1992), Joint inversion of fault zone head waves and direct P arrivals for crustal structure near major faults, *J. Geophys. Res.*, *97*, 1943–1951, doi:10.1029/91JB02748.

Blake, O. O., D. R. Faulkner, and A. Rietbrock (2013), The effect of varying damage history in crystalline rocks on the *P*- and *S*-wave velocity under hydrostatic confining pressure, *Pure Appl. Geophys.*, *170*(4), 493–505.

Calais, E., A. Freed, G. Mattioli, F. Amelung, S. Jónsson, P. Jansma, S.-H. Hong, T. Dixon, C. Prépetit, and R. Momplaisir (2010), Transpressional rupture of an unmapped fault during the 2010 Haiti earthquake, *Nat. Geosci.*, *3*, 794–799.

Cochran, E. S., and K. A. Kroll (2015), Stress- and structure-controlled anisotropy in a region of complex faulting—Yuha Desert California, *Geophys. J. Int.*, *202*, 1109–1121.

Cochran, E. S., Vidale, J. E., and Y.-G. Li (2003), Near-fault anisotropy following the Hector Mine earthquake, *J. Geophys. Res.*, *108*(B9), 2436, doi:10.1029/2002JB002352.

Chapman, C. H., and R. G. Pratt (1992), Traveltime tomography in anisotropic media: I. Theory, *Geophys. J. Int.*, *109*, 1–19.

Christensen, N. I., and D. A. Okaya (2007), Compressional and shear wave velocities in South Island, New Zealand rocks and their application to the interpretation of seismological models of the New Zealand crust, in *A Continental Plate Boundary: Tectonics at South Island, New Zealand*, edited by D. Okaya, T. Stern, and F. Davey, pp. 123–155, AGU, Washington, D. C.

Crampin, S. (1978), Seismic-wave propagation through a cracked solid: Polarization as a possible dilatancy diagnostic, *Geophys. J. R. Astron. Soc.*, *53*, 467–496.

Crampin, S. (1994), The fracture criticality of crustal rocks, *Geophys. J. Int.*, *118*, 428–438.

Davey, F. J. (2010), Crustal seismic reflection profile across the alpine fault and coastal plain at Whataroa, South Island, *N. Z. J. Geol. Geophys.*, *53*(4), 359–368.

Dempsey, E. D., D. J. Prior, E. Mariani, V. G. Toy, and D. J. Tatham (2011), Mica-controlled anisotropy within mid-to-upper crustal mylonites: An EBSD study of mica fabrics in the alpine fault zone, New Zealand, *Geol. Soc. London, Spec. Publ.*, *360*, 33–47.

Eberhart-Phillips, D., and S. Bannister 2002, Three-dimensional crustal structure in the Southern Alps region of New Zealand from inversion of local earthquake and active source data, *J. Geophys. Res.*, *107*(B10), 2262, doi:10.1029/2001JB000567.

Eccles, J. D., A. K. Gulley, P. E. Malin, C. M. Boese, J. Townend, and R. Sutherland (2015), Fault zone guided wave generation on the locked, late interseismic alpine fault, New Zealand, *Geophys. Res. Lett.*, *42*, 5736–5743, doi:10.1002/2015GL064208.

Evans, R. (1984), Anisotropy: A pervasive feature of fault zones? *Geophys. J. R. Astron. Soc.*, *76*, 157–163.

Faulkner, D. R., and E. H. Rutter (1998), The gas permeability of clay-bearing fault gouge at 20°C, *Geol. Soc. London, Spec. Publ.*, *147*, 147–156.

Faulkner, D. R., and E. H. Rutter (2000), Comparisons of water and argon permeability in natural clay-bearing fault gouge under high pressure at 20°C, *J. Geophys. Res.*, *105*, 16,415–16,426, doi:10.1029/2000JB900134.

Faulkner, D. R., and E. H. Rutter (2001), Can the maintenance of overpressured fluids in large strike-slip fault zones explain their apparent weakness?, *Geology*, *29*(6), 503–506.

Faulkner, D. R., A. C. Lewis, and E. H. Rutter (2003), On the internal structure and mechanics of large strike-slip fault zones: Field observations of the Carboneras fault in southeastern Spain, *Tectonophysics*, *367*(3–4), 235–251.

Ghorbani, A., M. Zamora, and P. Cosenza (2009), Effects of desiccation on the elastic wave velocities of clay-rocks, *Int. J. Rock Mech. Min. Sci.*, *46*, 1267–1272.

Gulley, A. K., J. D. Eccles, J. P. Kaipio, and P. E. Malin (2017), The effect of gradational velocities and anisotropy on fault-zone trapped waves, *Geophys. J. Int.*, *210*, 964–978.

Heap, M. J., and D. R. Faulkner (2008), Quantifying the evolution of static elastic properties as crystalline rock approaches failure, *Int. J. Rock Mech. Min. Sci.*, *45*, 564–573.

Hole, J. A., H. Thybo, and S. L. Klemperer (1996), Seismic reflections from the near-vertical San Andreas Fault, *Geophys. Res. Lett.*, *23*, 237–240, doi:10.1029/96GL00019.

Igel, H., G. Jahnke, and Y. Ben-Zion (2002), Numerical simulation of fault zone guided waves: accuracy and 3-D effects, *Pure Appl. Geophys.*, *159*, 2067–2083.

Jefferies, S. P., R. E. Holdsworth, C. A. J. Wibberley, T. Shimamoto, C. J. Spiers, A. R. Niemeijer, and G. E. Lloyd (2006), The nature and importance of phyllonite development in crustal-scale fault cores: An example from the median tectonic line, Japan, *J. Struct. Geol.*, *28*, 220–235.

Jeppson, T., and H. Tobin (2015), San Andreas fault zone velocity structure at SAFOD at core, log and seismic scales, *J. Geophys. Res. Solid Earth*, *120*, 4983–4997, doi:10.1002/2015JB012043.

Kaarsberg, E. (1959), Introductory studies of natural and artificial argillaceous aggregrates by sound propagation and X-ray diffraction methods, *J. Geol.*, *67*, 447–472.

Li, Y., P. Leary, K. Aki, and P. Malin (1990), Seismic trapped modes in the Oroville and San Andreas fault zones, *Science*, *249*, 763–766.

Lin, Y.-P., L. Zhao, and S.-H. Hung (2014), Full-wave multiscale anisotropy tomography in Southern California, *Geophys. Res. Lett.*, *41*, 8809–8817, doi:10.1002/2014GL061855.

Lin, G., and P. M. Shearer (2009), Evidence for water-filled cracks in earthquake source regions, *Geophys. Res. Lett.*, *36*, L17315, doi:10.1029/2009GL039098.

Liu, Y., T. Teng, and Y. Ben-Zion (2004), Systematic analysis of shear wave splitting in the aftershock zone of the 1999 Chi-Chi, Taiwan, earthquake: Shallow crustal anisotropy and lack of precursory variations, *Bull. Seismol. Soc. Am.*, *94*, 2330–2347.

Mitchell, T., and D. R. Faulkner (2009), The nature and origin of off-fault damage surrounding strike-slip fault zones with a wide range of displacements: A field study from the Atacama fault system, northern Chile, *J. Struct. Geol.*, *31*, 802–816.

Moore, D. E., and M. J. Rymer (2007), Talc-bearing serpentinite and the creeping section of the San Andreas fault, *Nature*, *448*, 795–797.

Peng, Z., Y. Ben-Zion, L. Zhu, and A. J. Michael (2003), Inference of a shallow fault zone layer in the rupture zone of the 1992 Landers, California earthquake from locations of events generating trapped waves and travel time analysis, *Geophys. J. Int.*, *155*, 1021–1041.

Quigley, M., R. Van Dissen, N. Litchfield, P. Villamor, B. Duffy, D. Barrell, K. Furlong, T. Stahl, E. Bilderback, and D. Noble (2012), Surface rupture during the 2010 M_w 7.1 Darfield (Canterbury) earthquake: Implications for fault rupture dynamics and seismic-hazard analysis, *Geology*, *40*(1), 55–58.

Rutter, E. H., R. H. Maddock, S. H. Hall, and S. H. White (1986), Comparative microstructures of natural and experimentally produced clay-bearing fault gouges, *Pure Appl. Geophys.*, *124*(1), 3–30.

Rutter, E. H., D. R. Faulkner, and R. Burgess (2012), Structure and geological history of the Carboneras fault zone, SE Spain: Part of a stretching transform fault system, *J. Struct. Geol.*, *45*, 68–86.

Savage, M., W. Peppin, and U. Vetter (1990), Shear wave anisotropy and stress direction in and near Long Valley caldera, California, *J. Geophys. Res.*, *95*, 11,165–11,117, doi:10.1029/JB095iB07p11165.

Taylor, R., E. H. Rutter, S. E. J. Nippress, and K. H. Brodie (2015), Seismic velocity modelling of the Carboneras fault zone, SE Spain, *Tectonophysics*, *646*, 20–35.

Thurber, C., H. Zhang, F. Waldhauser, J. Hardebeck, A. Michael, and D. Eberhart-Philips (2006), Three-dimensional compressional wavespeed model, earthquake relocations, and focal mechanisms for the Parkfield, California, region, *Bull. Seismol. Soc. Am.*, *96*, S38–S49.

Williams, J. N., V. G. Toy, C. Massiot, D. D. McNamara, and T. Wang (2016), Damaged beyond repair? Characterising the damage zone of a fault late in its interseismic cycle, the Alpine Fault, New Zealand, *J. Struct. Geol.*, *90*, 76–94.

Yan, Z., R. W. Clayton, and J. Saleeby (2005), Seismic refraction evidence for steep faults cutting highly attenuated continental basement in the central transverse ranges, California, *Geophys. J. Int.*, *160*, 651–666.

Zhang, H., Y. Liu, C. Thurber, and S. Roecker (2007), Three-dimensional shear-wave splitting tomography in the Parkfield, California, region, *Geophys. Res. Lett.*, *34*, L24308, doi:10.1029/2007GL031951.